*Anal. Bioanal. Electrochem., Vol. 10, No. 8, 2018, 961-973*

**Analytical & Bioanalytical Electrochemistry**

2018 by CEE
www.abechem.com

*Full Paper*

# One-step Electrophoretic/electrochemical Synthesis of Reduced Graphene Oxide/Manganese Oxide (rGO-$Mn_3O_4$) Nanocomposite and Study of its Capacitive Performance

**Mustafa Aghazadeh**

*Materials and Nuclear Research School, Nuclear Science and Technology Research Institute (NSTRI), P.O. Box 14395-834, Tehran, Iran*

E-Mail: maghazadeh@aeoi.org.ir

*Received: 20 September 2017 / Received in revised form: 3 May 2018 / Accepted: 25 June 2018 / Published online: 31 August 2018*

**Abstract**- Herein, a very simple and scalable electrochemical strategy is reported to fabricate reduced graphene oxide (rGO)-$Mn_3O_4$ nanoparticles composite for supercapacitors. First, graphene oxide is directly produced via Hummers method, and dispersed in manganese nitrate aqueous solution. The rGO-$Mn_3O_4$ particles nanocomposite is then prepared through electrochemically decoration of $Mn_3O_4$ nanoparticles onto reduced graphene oxide (rGO) sheets. The formation of composite is explained by electrophoretic/electrochemical deposition (EPD/ECD) mechanism. The as-prepared rGO-$Mn_3O_4$ nanocomposite is characterized by XRD, IR, FE-SEM and TEM techniques. These analyses results specified the co-deposition of manganese oxide particles and rGO sheets on the cathode electrode. The charge storage ability of the fabricated nanocomposite as electrode material for supercapacitors was studied using cyclic voltammetry and charge-discharge techniques. The obtained electrochemical data indicated that the rGO-$Mn_3O_4$ nanocomposite enable to provide specific capacitance of 364 F $g^{-1}$ at 2 A $g^{-1}$ and 86.3% of its initial capacity after 5000 charge/discharging.

**Keywords-** rGO-$Mn_3O_4$ nanocomposite, Nanoparticles, Graphene oxide, Electrochemical synthesis

## 1. INTRODUCTION

Supercapacitors (SCs) have recently gained significant attention due to their excellent charge–discharge performance, long-term cycle life, and high power densities [1]. Furthermore, SCs could also make up the difference in energy and power between batteries and traditional capacitors. It was reported that transition metal oxides (TMOs) will play a significant role in developing the low-cost and high-powered supercapacitors [2]. Furthermore, compositing the nanostructured TMOs with carbon-based materials could remarkably improve the SC properties of TMOs [3]. In this regard, it has been clearly verified that the metal oxides like as nickel oxide [4-6], cobalt oxide [7-9], iron oxide [10-15] and manganese oxide [16-19] are promising materials for use in SCs as compared with other TMOs. Furthermore, manganese dioxides ($MnO_2$ and $Mn_3O_4$) have attracted much attention for its good electrochemical capacitive properties, wide potential range, low cost, and environmental friendliness [20,21]. However, the low electrical conductivity of manganese oxides ($10^{-5}$–$10^{-6}$ S/cm) lead to its poor electrochemical capability in energy storage applications like batteries and capacitors [22]. It has been reported that wrapping or decoration of manganese oxide onto a conductive substrates could overcome the mentioned problem to a certain extent. Until now, various conductive networks including activated carbon [23-25], carbon particles [26], carbon nanotubes [27-29], carbon fiber [30,31], nickel foam [32], metal ion doping [33], graphene [34-38], graphene oxide [39,40] and reduced GO [41-46] have been applied to load manganese oxide, which has been resulted an increasing conductivity and restricting volume change during GCD process. Combining manganese oxides with graphene-based networks could improve the electrical conductivity and stability of the fabricated electro-active materials, and enhance its electrochemical performances [34-43]. Among the graphene-based conductive material used for preparation of manganese oxide composites, reduced graphene oxide sheet (rGO) is reported to be a more suitable one as compared with conductive polymers due to its prominent advantages of high conductivity and stability [44-46]. However, the mass loading of oxide material onto the carbon-based network is steel major problem. In some work, layer by layer deposition of composite component has been proposed and it has been observed that the low conductivity problem could be effectively refined [47,48]. Herein we developed an electrochemical/electrophoretic approach for simultaneously formation of rGO/manganese oxide composite, where the highest contact between carbon-based network and oxide part of composite could be provided and the excellent electrochemical performance is expected. The cathodic electrochemical synthesis strategy is used for decoration of manganese oxide onto rGo sheets. Cathodic electrochemical synthesis has been considered as powerful method for synthesis of various TMOs [49-59]. However, this route has been rarely used for fabrication of TMOs/graphene composites [60-62]. Electrophoretic deposition (EPD) is also applied as a facile route for composite synthesis [63,64]. Here, we used co-deposition of GO and manganese oxide through EPD and ECD,

respectively, for the fabrication of rGO-$Mn_3O_4$ nanocomposite. To the best of our knowledge, preparation of rGO-$Mn_3O_4$ composite has not been reported through this method. The crystal phase, chemical structure, morphology and electrochemical properties of the prepared composite were investigated by XRD, IR, FE-SEM, TEM, cyclic voltammetry (CV) and galvanostatic charge-discharge (GCD) techniques. The results verified the successful preparation of the mentioned composite *via* simultaneous EPD-ECD strategy.

## 2. EXPERIMENTAL PROCEDURE

### 2.1. Materials

Mn nitrate tetrahydrate ($Mn(NO_3)_2 \cdot 4H_2O$, 99.5%), $Na_2SO_4$ were purchased from Sigma Aldrich. Graphene oxide (GO) was provided from Research Institute of Petroleum Industry (IRIP). All materials were used as received, without any purification.

### 2.2. Synthesis of rGO-$Mn_3O_4$ composite

For the synthesis of $Mn_3O_4$/rGO composite, electrophoretic deposition/electrochemical deposition techniques were used. Electrochemical set up includes an electrochemical cell containing deposition electrolyte and a home-made electrochemical workstation system (Potentiostat/Galvanostat, Model: NCF-PGS 2012, Iran). The cell electrodes were a steel sheet (surface area of 1 $cm^2$) centered between two parallel graphite anodes. The deposition time and bath temperature were 20 min and 25 $^oC$, respectively. An aqueous electrolyte was prepared as follow; First, 0.2 g graphene oxide powder was dispersed in 100 cc deionized water by assisted of probe sonicator. Then, 0.8 g manganese nitrate was added into graphene oxide dispersed solution and stirred for 30 min. This prepared electrolyte was used as the electrodeposition bath in the synthesis of rGO-$Mn_3O_4$ composite. To deposition of the rGO-$Mn_3O_4$ composite onto steel grid, current density of 5 mA $cm^{-2}$ was applied into the prepared electrolyte for 30min. After deposition, the steel sheet was washed several times with the deionized $H_2O$ and dried at 70 $^oC$ for 1h. The fabricated electrode (rGO-$Mn_3O_4$@steel sheet) was directly used as working electrode in the capacitance measurement tests. Furthermore, the deposited composite film was scrapped and used in powder form for structural characterization through XRD, IR, SEM and TEM analyses.

### 2.3. Instruments

Morphologies of the synthesized composite powder were observed through field-emission scanning electron microscopy (FE-SEM, Mira 3-XMU with accelerating voltage of 100 kV). The crystal phase of the prepared composite was specified by X-ray diffraction (XRD, Phillips PW-1800) using a Co Kα radiation. Transmission electron microscopy (TEM, model

Zeiss EM900 with an accelerating voltage of 80 kV) was used to provide high resolution images. The chemical bonds in the prepared composite were studied through FTIR spectroscopy using model Bruker Vector 22 FT-IR spectrometer.

### 2.4. Electrochemical evaluations

The electrochemical evaluations were carried out on a AUTOLAB® (Eco Chemie, PGSTAT 30) electrochemical analyzer in a three-electrode system. The working electrode was the synthesized rGO-$Mn_3O_4$@steel sheet with mass loading of 3 mg. A conventional three-electrode system, containing the working electrode, Pt counter electrode and Ag/AgCl reference electrode was assembled to perform electrochemical evaluations. First, electrochemical experiments were done in a conventional three-electrode cell with 1 M $Na_2SO_4$ electrolyte. The capacitance performance of the prepared composite electrode was characterized by using cyclic voltammetry (CV) and galvanostatic charge-discharge techniques. The CVs of the fabricated composite electrode were performed in the potential window of 0 to +0.9 V *vs*. Ag/AgCl at the potential sweeps of 5, 10, 25, 50 and 100 mV $s^{-1}$. The charge-discharge diagrams were recorded at the different currents of 0.5, 1, 2, 3 and 5 A $g^{-1}$ within a potential range of 0 to +0.9V *vs*. Ag/AgCl. The specific capacitances (Cs) of the fabricated composite were calculated from the applied techniques i.e. from Eq. (1) using CV data and from Eq. (2) using GCD data [65]:

$$\mathrm{Cs(F\ g^{-1})} = \frac{\mathrm{Q}}{\mathrm{m\Delta\ (V)}},\ \ \mathrm{Q} = \int_{\mathrm{V_a}}^{\mathrm{V_a}} I(V)dV \qquad (1)$$

Where Cs is the specific capacitance (F/g), *m* is the mass of the electrode (g), *v* is the scan rate of CV curves (V/s), and (Va− Vc) represents the potential window (V) [66].

$$Cs\ (F\ g^{-1}) = \frac{Q}{m\times\Delta V}\ , Q = I \times \Delta t \qquad (2)$$

Where Cs is the specific capacitance (F/g), I is the current load (A), m is the composite mass load onto the steel sheet (g), ΔV is the applied potential range (V), and Δt is the discharge time (s).

## 3. RESULTS AND DISCUSSION

### 3.1. Structural and morphological characterizations

The X-ray diffraction patterns of the graphene oxide powder and the electro-synthesized composite is presented in Fig. 1. The characteristic diffraction peak of GO is observed at the 2thetha of 9.5 degree (Fig. 1a). In the pattern of composite (Fig. 1b), all the observed diffraction peaks are correspond to the crystalline hausmannite ($Mn_3O_4$) (JCPDS 01-1127)

[67]. Moreover, the peak for the graphene oxide sheets is almost disappeared, suggesting that the rGO sheets in the rGO-$Mn_3O_4$ nanocomposite are stacked in a disordered manner [68]. These results indicate that the fabricated rGO-$Mn_3O_4$ nanocomposite is composed of $Mn_3O_4$ nanoparticles and disorderedly stacked rGO nanosheets.

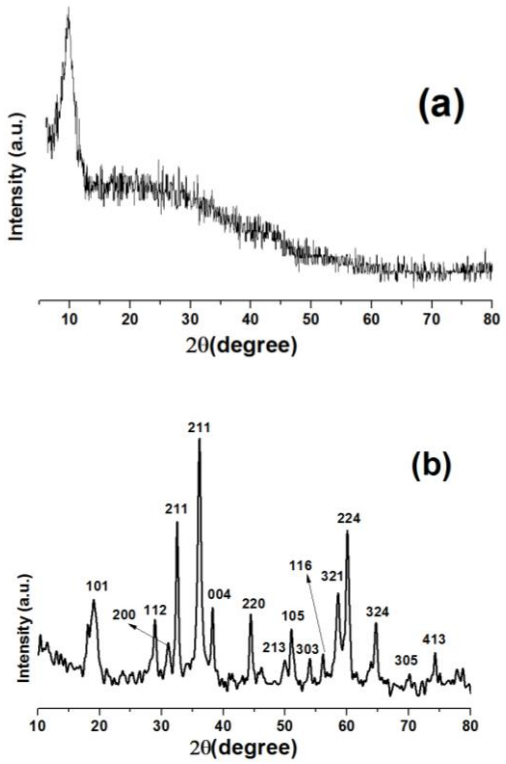


**Fig. 1.** XRD patterns of (a) GO powder and (b) the electro-synthesized rGO-$Mn_3O_4$ composite

FT-IR spectra of the GO and its composite with manganese oxide are presented in Fig. 2. In the spectrum of GO, a strong and broad absorption at 3429 $cm^{-1}$ due to O–H stretching vibration of carboxyl groups and the absorbed water. The peaks at 1403 and 1274 $cm^{-1}$ correspond to the skeletal vibrations of C–OH and C–O–C [42,69]. The characteristic peak for C=O stretching vibration appears at 1723 $cm^{-1}$[69,44]. The peak at 1632 $cm^{-1}$ corresponds to C=C skeletal stretching vibration. The stretching peak appears at 2922 $cm^{-1}$ and 1462 $cm^{-1}$ are attributable to C–H and C–C band, which refer to skeletal vibrations of non-oxidized graphitic domains [42]. The presense of peak at 1588 $cm^{-1}$ belong to C=O group band could be assigned to the unreduced –C=OH group. The peak at 1061 $cm^{-1}$ suggested C–O vibrations of carboxylic acid [44]. In the spectrum of the compsoite (Fig. 2b), the new IR bands (at 490 $cm^{-1}$ and 620 $cm^{-1}$) are observed, which are due to Mn–O stretching mode in tetrahedral and octahedral sites [42,44]. Furthermore, the absorption band at 3459 $cm^{-1}$ is due to the O–H vibrations from adsorbed moisture. Notably, the peak relating to the C=O groups is not apperead in FTIR spectrum of the composite nanocomposites, confirming that GO is reduced

to rGO during the electrochemical depsotion of $Mn_3O_4$. These results verified the sucsessful synthesis of rGO-$Mn_3O_4$ composite though EPD-ECD method.

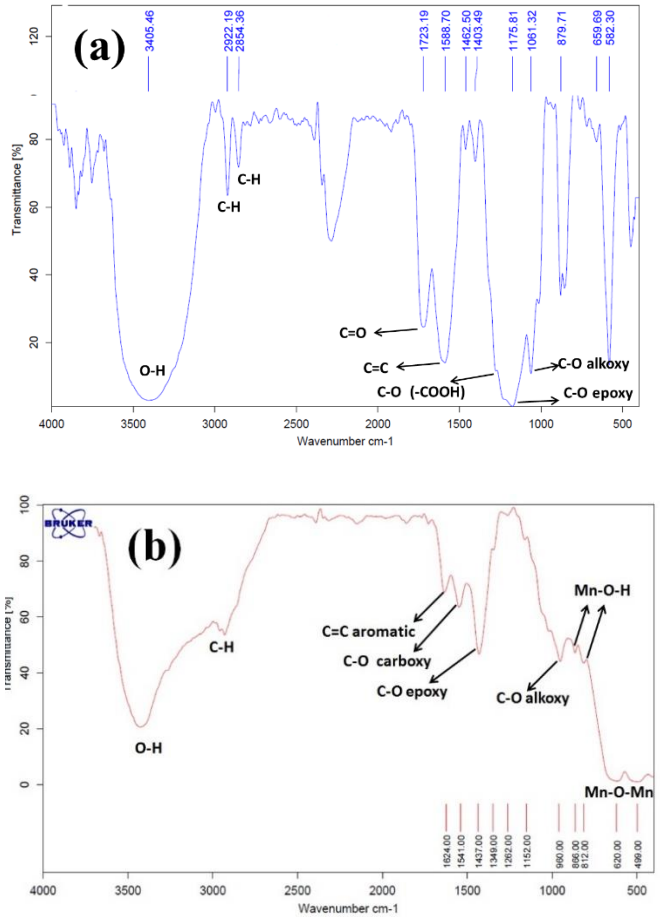


**Fig. 2.** IR spectra of (a) GO and (b) rGO-$Mn_3O_4$ composite

The morphology of the fabricated composite is given in Figs. 3a and b. For the prepared composite, two types of morphologies (i.e. particle and sheet) are seen in the FE-SEM images. The sheet-like texture is assigned to the reduced graphene oxide part of the composite and the particle one is indicate the electrochemically grown $Mn_3O_4$ deposits onto the rGO sheets (Fig. 3a). In fact, these observations suggested that $Mn_3O_4$ nanoparticles are intimately anchored on the rGO sheets. Furthermore, the surfaces of rGO sheets are fully filled by $Mn_3O_4$ nanoparticles, as shown in Fig. 3b. The energy-dispersive X-ray (EDS) data of the composite is also given in Fig. 3c. The presence of 19.68%wt Mn, 64.25%wt O, and 16.08%wt C elements are observed, which fully proved the $Mn_3O_4$ and rGO components in the fabricated composite. As observed in Fig. 3b, the oxide particles are decorated onto the rGO sheets. This fact suggested that the electrochemical grown of manganese oxide NPs is occurred on the electrophoretically deposited rGO sheets onto the cathode surface. Hence, an

EPD-ECD mechanism was proposed for the formation of rGO-$Mn_3O_4$ composite on the cathode electrode. The schematic view of the proposed mechanism is presented in Fig. 4.

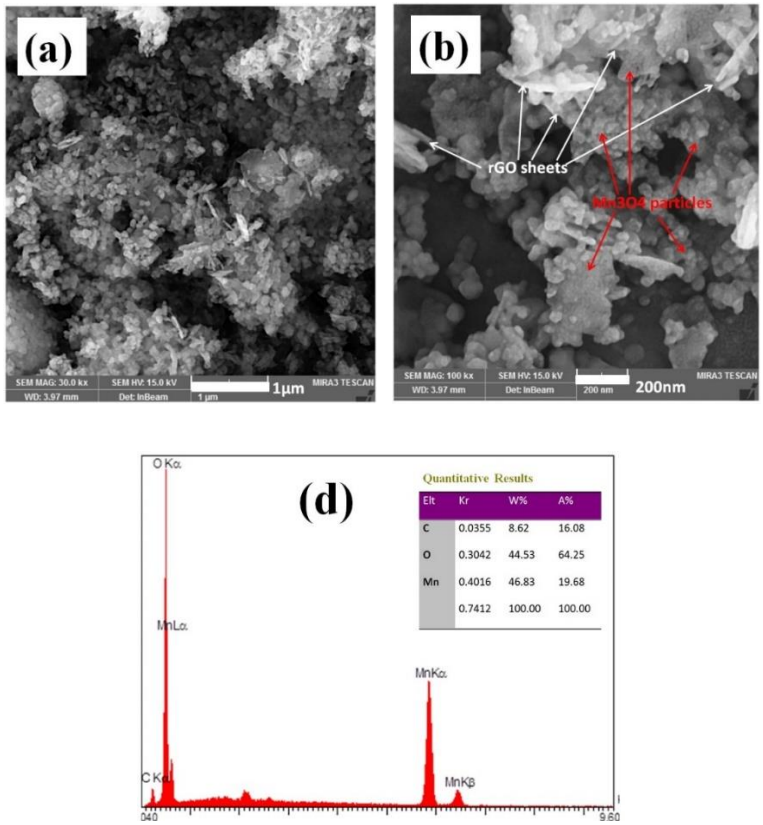


**Fig. 3.** (a,b) FE-SEM images the electro-synthesized rGO-$Mn_3O_4$ composite and (c) its EDS data

First, GO sheets dispersed in water electrolyte through negatively charged carboxylic groups are electrophoretically deposited into the cathode surface as shown in Fig. 4a. Notably, the metal ions ($Mn^{2+}$) connected to the negatively charged $COO^-$ groups of GO are also moved to the cathode surface together with the GO sheets, as seen in Fig. 4a. As the GO sheet receive to the cathode surface, the formation and deposition $Mn_3O_4$ particle is occurred on the cathode surface (Fig. 4b). Furthermore, the reduction of GO is also taken placed at the high basic condition on the cathode surface. In final, composition of rGO-$Fe_3O_4$ nanoparticles are formed on the cathode (Fig. 4b), which are completely verified through TEM observations (Fig. 5). For the electrodeposited pristine iron oxide, TEM observations revealed particle morphology with average diameter of 10 nm (Fig. 5a). For the composite, well dispersed thin rGO sheets are clearly observed where iron oxide particles (diameter≈15 nm) are present on their surfaces (Fig. 5b). This arrangement of oxide NPs onto rGO sheet prevents their agglomeration since iron oxide NPs tend to stick each other as a result of their magnetic character, where the agglomerated particles were observed for the pristine $Fe_3O_4$

NPs (Fig. 5a). TEM images in Fig. 5 indicated that the $Mn_3O_4$ NPs (with sizes of 10 nm) have been formed onto the rGO sheets.

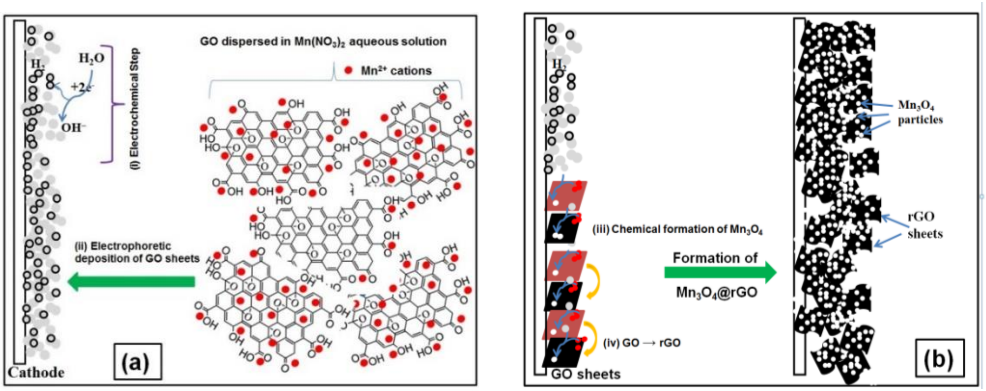


**Fig. 4.** Formation mechanism of rGO-$Mn_3O_4$ composite

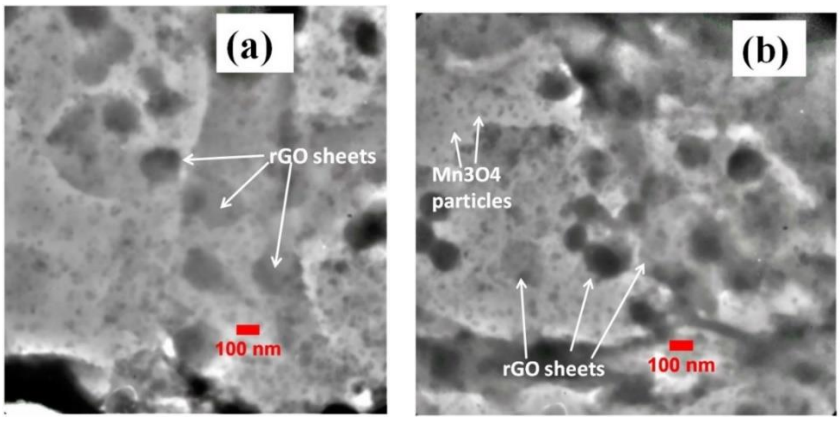


**Fig. 5.** TEM images of the prepared GO-$Mn_3O_4$ composite

### 3.2. Capacitance measurments

The electrochemical performance of the fabricated rGO-$Mn_3O_4$ nanocomposite was first studied using cycle voltammetry in 1 M $Na_2SO_4$ electrolyte at a potential window of 0-0.9 V. As seen in Fig. 6a, the fabricated rGO-$Mn_3O_4$ electrode have nearly rectangle-shaped and symmetric CV curves without any redox peak currents at all the applied scan rates, suggesting the ideal capacitive nature [43,44]. The CV current response of the fabricated increases gradually with the increase of scan rate and no significant change in the shape of CV curve even at high scan rates, indicating an excellent capacitance behavior and the fast diffusion of electrolyte ions into the fabricated rGO-$Mn_3O_4$ electrode. Using Eq. (1), the capacitances at 5, 10, 25, 50 and 100 mV/s were calculated to be 454, 419, 378, 344 and 302 F/g, respectively.

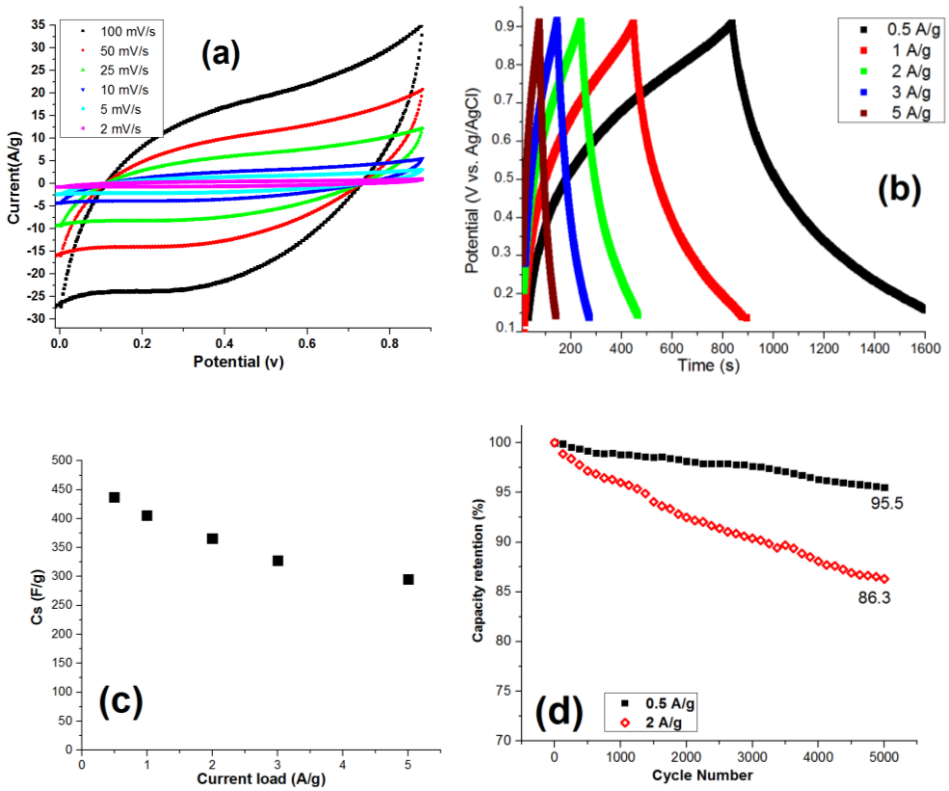


**Fig. 6.** (a) cyclic voltammograms; (b) charge-discharge; (c) the calculated capacitance values and (d)cycling stability for the fabricated rGO-$Mn_3O_4$ electrode

Fig. 6b indicates the charge-discharge profiles of the fabricated electrode at various current densities over the potential range of 0-0.9 V. No obviously shape change was observed among the nearly linear GCD curves at all applied current loads, implicating the good rate capability and reversibility. The charge/discharge time varies at a constant current density for $Mn_3O_4$/rGO electrode, suggesting different Cs values. As shown in Fig. 6c, the Cs values of rGO-$Mn_3O_4$ nanocomposite electrode were calculated to be 438, 405, 364, 329 and 297 F/g at 0.5, 1, 2, 3 and 5 A/g, respectively, which is higher than the reported Cs values for pristine nanostructured $Mn_3O_4$ and its composite electrode in the literature; e.g. 210 F/g for nanostructured $Mn_3O_4$ at 0.5 A/g [16], 298 F/g for $Mn_3O_4$ nanorods at 1 A/g [17], 279 F/g for vertically-aligned $Mn_3O_4$ nanorods at 1 A/g [19], 293 F/g for $Mn_3O_4$ nanorods/Ni foam at 0.5 A/g [32], 272 F/g for Cr-doped $Mn_3O_4$ nanocrystals at 0.5 A/g [33], 258.6 F/g for $Mn_3O_4$/rGO nanocomposite at 0.25 A/g [41], 342.5 F/g for $Mn_3O_4$/rGO electrode at 1 A/g [42], 125 F/g for rGO/$Mn_3O_4$ composite at 1 A/g [44], 457 F/g for rGO-$Mn_3O_4$ at 1 A/g [45], 207.2 F/g for $Mn_3O_4$/rGO at 1 A/g [46], and 194.5 F/g for $Mn_3O_4$/RGO-0.35 electrode at 0.5 A/g [70]. These enhancements signified the positive synergistic corporation between reduced graphene oxide and hausmannite which may originate from the following issues: (a) uniformly anchoring the $Mn_3O_4$ particles on reduced graphene oxide sheets (as confirmed by TEM observations in Fig. 5), (b) reduced graphene oxide sheets provides the highly conductive electronic network for the redox process of electrode, (c) incorporation of $Mn_3O_4$

particles into the reduced graphene oxide sheets could finish the re-stacking of reduced graphene oxide sheets, and (d) reduced graphene oxide could prevents the volume change and agglomeration of oxide during GDC process. These events maximize the following cases; (i) interface area between $Mn_3O_4$ particles and reduced graphene oxide sheets, (ii) the electrochemical usage of electro-active materials, and (iii) ionic, electrical and charge transfer pathways. The above mentioned charterers of rGO-$Mn_3O_4$ nanocomposite give it to exhibit the observed supercapacitive performances.

The fabricated composite electrode was cycled 5000 times at the currents of 0.5 and 2 A $g^{-1}$, and the calculated capacity retention values are shown in Fig. 5d. It was observed that the fabricated electrode could be deliver 95.5% and 86.3% of its initial capacity after 5000 times cycling at current of 0.5 and 2 A $g^{-1}$. These data specified the suitable cycling performance of the composite.

## 4. CONCLUSION

In summary, rGO-$Mn_3O_4$ nanocomposite was successfully synthesized through a mixed electrophoretic/electrochemical deposition approach. Highly dispersed $Mn_3O_4$ nanoparticles with a size of 10 nm were in situ deposited on the surface of rGO sheets with uniform particle distribution. The prepared rGO-$Mn_3O_4$ nanocomposite were used as electrode materials for supercapacitor. It was observed that the fabricated rGO-$Mn_3O_4$ nanocomposite is enable to deliver greatly enhanced capacitive performance and long-term stability. Based on the obtained results, the one-pot EPD/ECD procedure is proposed as facile synthesis method for fabrication of binder-free oxide/reduced graphene electrodes for supercapacitor uses.

## REFERENCES

[1] F. Wang, X. Wu, X. Yuan, Z. Liu, Y. Zhang, L. Fu, Y. Zhu, Q. Zhou, Y. Wu, and W. H. Chem. Soc. Rev. 46 (2017) 6816.

[2] D. P. Dubal, O. Ayyad, V. Ruiz, and P. Gómez-Romero Chem. Soc. Rev. 44 (2015) 1777.

[3] G. Zhang, X. Xiao, B. Li, P. Gu, H. Xue, and H. Pang, J. Mater. Chem. A 5 (2017) 8155.

[4] M. Aghazadeh, J. Mater. Sci.: Mater. Electron. 28 (2016) 3108.

[5] M. Aghazadeh, and M. R. Ganjali, J. Mater. Sci.: Mater. Electron.28 (2017) 8144.

[6] M. Aghazadeh, A. Rashidi, and M. R. Ganjali, Int. J. Electrochem. Sci. 11 (2016) 11002.

[7] M. Aghazadeh, J. Appl. Electrochem. 42 (2012) 89.

[8] M. Aghazadeh, R. Ahmadi, D. Gharailou, M. R. Ganjali, and P. Norouzi, J. Mater. Sci.: Mater. Electron. 27 (2016) 8623.

[9] M. Aghazadeh, M. Hosseinifard, B. Sabour, and S. Dalvand, Appl. Surf. Sci. 287 (2013) 187.
[10] M. Aghazadeh, I. Karimzadeh, and M. R. Ganjali, J. Mater. Sci.: Mater. Electron. 28 (2017) 13532.
[11] M. Aghazadeh, J. Mater. Sci.: Mater. Electron. 28 (2017) 18755.
[12] M. Aghazadeh, and M. R. Ganjali, J. Mater. Sci. 53 (2018) 295.
[13] M. Aghazadeh, I. Karimzadeh, M. R. Ganjali, and A. Behzad, J. Mater. Sci.: Mater. Electron. 28 (2017) 18121.
[14] M. Aghazadeh, and M. R. Ganjali, Ceram. Int. 44 (2018) 520.
[15] M. Aghazadeh, I. Karimzadeh, M. Ghannadi Maragheh, and M. R. Ganjali, Korean J. Chem. Engin. 35 (2018) 1341.
[16] Z. Qi, A. Younis, D. Chu, and S. Li, Nano-Micro Lett. 8 (2016) 165.
[17] M. Aghazadeh, A. Bahrami-Samani, D. Gharailou, M.G. Maragheh, and M. R. Ganjali, J. Mater. Sci.: Mater. Electron. 27 (2016) 11192.
[18] M. Aghazadeh, M. R. Ganjali, and P. Norouzi, J. Mater. Sci.: Mater. Electron. 27 (2016) 7707.
[19] M. Aghazadeh, M. R. Ganjali, and P. Noruzi, Thin Solid Films 634 (2017) 24.
[20] W. F. Wei, X. W. Cui, W. X. Chen, and D. G. Ivey, Chem. Soc. Rev. 40 (2011) 1697.
[21] T. Kou, B. Yao, T. Liu, and Y. Li, J. Mater. Chem. A 5 (2017) 17151.
[22] T. Zhai, X. Lu, F. Wang, H. Xia, and Y. Tong, Nanoscale Horiz. 1 (2016) 109.
[23] X. Xiao, Y. Wang, G. Chen, L. Wang, and Y. Wang, J. Alloys Compd. 703 (2017) 163.
[24] C. Liu, H. Song, C. Zhang, Y. Liu, C. Zhang, X. Nan, and G. Cao, Nano Res. 8 (2015) 3372.
[25] L. Xu, M. Jia, Y. Li, X. Jin, and F. Zhang, Sci. Rep. 7 (2017) 12857.
[26] S. Nagamuthu, S. Vijayakumar, and G. Muralidharan, Energy Fuels 27 (2013) 3508.
[27] Y. Z. Song, R. X. Zhao, K. K. Zhang, J. J. Ding, X. M. Lv, M. Chen, and J. M. Xie, Electrochim. Acta 230 (2017) 350.
[28] M. Mandal, D. Ghosh, K. Chattopadhyay, and C. K. Das, J. Electron. Mater. 45 (2016) 491.
[29] H. Z. Chi, S. Tian, X. Hu, H. Qin, and J. Xia, J. Alloys Compd. 587 (2014) 354.
[30] H. Cheng, H. M. Duong, and D. Jewell, RSC Adv. 6 (2016) 36954.
[31] H. Wang, C. Xu, Y. Chen, and Y. Wang, Energy Storage Mater. 8 (2017) 127.
[32] D. Li, F. Meng, X. Yan, L. Yang, H. Heng, and Y. Zhu, Nanoscale Res. Lett. 8 (2013) 535.
[33] R. Dong, Q. Ye, L. Kuang, X. Lu, Y. Zhang, X. Zhang, G. Tan, Y. Wen, and F. Wang, ACS Appl. Mater. Interfaces 5 (2013) 9508.
[34] Y. Tian, D. Li, J. Liu, H. Wang, J. Zhang, Y. Zheng, T. Liu, and S. Hou, Electrochim. Acta 257 (2017) 155.

[35] A. E. Rashedab, A. A. El-Moneim, Mater. Today energy 3 (2017) 24.
[36] X. Qiu, D. Xu, L. Ma, and Y. Wang, Int. J. Electrochem. Sci. 12 (2017) 2173.
[37] S. Hassan, M. Suzuki, and A. Abd El-Moneim, Int. J. Electrochem. Sci. 9 (2014) 8340.
[38] C. Xiong, T. Li, M. Khan, H. Li, and T. Zhao, RSC Adv. 5 (2015) 85613.
[39] Y. Wang, J. Mater. Res. 30 (2015) 4.
[40] F. Ding, N. Zhang, C. Zhang, and C. Zhang, Mater. Transactions 56 (2015) 1857.
[41] J. Xu, X. Fan, Q. Xia, Z. Shao, B. Pei, Z. Yang, Z. Chen, and W. Zhang, J. Alloys Compd. 685 (2016) 949.
[42] Y. Zhou, L. Guo, W. Shi, X. Zou, B. Xiang, and S. Xing, Mater. 11 (2018) 881.
[43] T. Xiong, W. Siang, V. Lee, X. Huang, and J. M. Xue, J. Mater. Chem. A 5 (2017) 12762.
[44] X. She, X. Zhang, J. Liu, L. Lia, X. Yu, Z. Huang, and S. Shang, Mater. Res. Bull. 70 (2015) 945.
[45] H. U. Shaha, F. Wang, M. Sufyan Javed, N. Shaheen, M. Saleemd, and Y. Lia, Ceram. Int. 44 (2018) 3580.
[46] P. Rosaiah, J. Zhu, D. P. M. D. Shaik, O. M. Hussain, Y. Qiu, and L. Zhao, J. Electroanal. Chem. 794 (2017) 78.
[47] H. Jiang, L. Yang, C. Li, C. Yan, P. S. Lee, and J. Ma, Energy Environ. Sci. 4 (2011) 1813.
[48] J. Shin, D. Shin, H. Hwang, T. Yeo, S. Park, and W. Choi, J. Mater. Chem. A 5 (2017) 13488.
[49] M. Aghazadeh, A. N. Golikand, M. Ghaemi, and T. Yousefi, J. Electrochem. Soc. 158 (2011) E136.
[50] T. Yousefi, A. N. Golikand, M. H. Mashhadizadeh, and M. Aghazadeh, J. Taiwan Institute Chem. Eng. 43 (2012) 614.
[51] M. Aghazadeh, Mater. Lett. 211 (2018) 225.
[52] M. Aghazadeh, M. G. Maragheh, M. R. Ganjali, and P. Norouzi, RSC Adv. 6 (2016) 10442.
[53] M. Aghazadeh, A. Nozad, H. Adelkhani, and M. Ghaemi, J. Electrochem. Soc. 157 (2010) D519.
[54] M. Aghazadeh, M. Ghaemi, A. N. Golikand, and A. Ahmadi, Mater. Lett. 65 (2011) 2545.
[55] I. Karimzadeh, H. R. Dizaji, and M. Aghazadeh, J. Magn. Magn. Mater. 416 (2016) 81.
[56] M. Aghazadeh, A. A. M. Barmi, H. M. Shiri, and S. Sedaghat, Ceram. Int. 39 (2013) 1045.
[57] M. Aghazadeh, A. A. M. Barmi, and M. Hosseinifard, Mater. Lett. 73 (2012) 28.
[58] M. Aghazadeh, M. G. Maragheh, M. R. Ganjali, and P. Norouzi, Inorg. Nano-Metal Chem. 27 (2017) 1085.

[59] F. Khosrow-pour, M. Aghazadeh, and B. Arhami, J. Electrochem. Soc. 160 (2013) D150.
[60] Rusi, and S. R. Majid, Scientific Reports 5 (2015) 16195.
[61] S. Ghasemi, R. Hosseinzadeh, and M. Jafari, Int. J. Hydrogen Energy 40 (2015) 1037.
[62] Y. Zhao, D. Zhao, P. Tang, Y. Wang, C. Xu, and H. Li, Mater. Lett. 76 (2012) 127.
[63] A. Chavez-Valdez, M. S. P. Shaffer, and A. R. Boccaccini, J. Phys. Chem. B 117 (2013) 1502.
[64] M. Diba, D. W. H. Fam, A. R. Boccaccini, and M. S. P. Shaffer, Prog. Mater. Sci. 82 (2016) 83.
[65] M. Aghazadeh, and M. R. Ganjali, J. Mater. Sci.: Mater. Electron. 28 (2017) 11406.
[66] M. Aghazadeh, I. Karimzadeh, and M. R. Ganjali, Mater. Lett. 209 (2017) 450.
[67] R. Cheraghali, and M. Aghazadeh, Anal. Bioanal. Electrochem 8 (2016) 193.
[68] S. Chen, J. W. Zhu, X. D. Wu, Q. F. Han, and X. Wang, ACS Nano 4 (2010) 2822.
[69] T. Wang, Y. Li, S. Geng, C. Zhou, X. Jia, F. Yang, L. Zhang, X. Ren, and H. Yang, RSC Adv. 5 (2015) 88958.
[70] Y. Wang, Z. Ji, X. Shen, K. Xu, and A. Yuan, J. Alloys Compd. 684 (2016) 366.